Front. Environ. Sci. Eng. 2018, 12(2): 15
https://doi.org/10.1007/s11783-018-1017-z

RESEARCH ARTICLE

Abatement of mixed volatile organic compounds in a catalytic hybrid surface/packed-bed discharge plasma reactor

Lianjie Guo[1,3], Nan Jiang[1,2,3], Jie Li (✉)[1,2,3], Kefeng Shang[1,2,3], Na Lu[1,2,3], Yan Wu[1,2,3]

1 Key Laboratory of Industrial Ecology and Environmental Engineering (Ministry of Education), Dalian University of Technology, Dalian 116024, China
2 School of Electrical Engineering, Dalian University of Technology, Dalian 116024, China
3 School of Environmental Science & Technology, Dalian University of Technology, Dalian 116024, China

HIGHLIGHTS

- Mixed VOCs were successfully degraded by HSPBD reactor with Ag-Ce/γ-Al_2O_3 catalyst at room temperature.
- The removal performance of single-component and mixed VOCs were compared in both NTP and PPC processes.
- The single-component and mixed VOCs decomposition products after plasma-catalysis treatment were analyzed.
- There existed an optimal gas humid to achieve the highest mixed VOCs removal efficiency.

GRAPHIC ABSTRACT

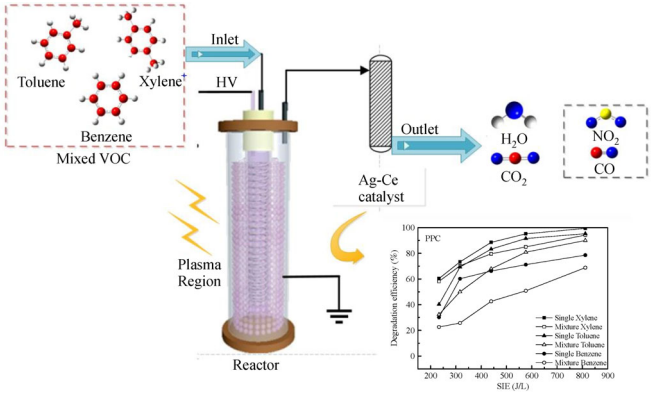

ARTICLE INFO

Article history:
Received 4 March 2017
Revised 4 September 2017
Accepted 1 December 2017
Available online 18 January 2018

Keywords:
Mixed VOCs
HSPBD plasma reactor
Degradation
Catalyst
Relative humidity

ABSTRACT

In this study, post plasma-catalysis degradation of mixed volatile organic compounds (benzene, toluene, and xylene) has been performed in a hybrid surface/packed-bed discharge plasma reactor with Ag-Ce/γ-Al_2O_3 catalyst at room temperature. The effect of relative air humidity on mixed VOCs degradation has also been investigated in both plasma-only and PPC systems. In comparison to the plasma-only system, a significant improvement can be observed in the degradation performance of mixed VOCs in PPC system with Ag-Ce/γ-Al_2O_3 catalyst. In PPC system, 68% benzene, 89% toluene, and 94% xylene were degraded at 800 $J \cdot L^{-1}$, respectively, which were 25%, 11%, and 9% higher than those in plasma-only system. This result can be attributed to the high catalytic activity of Ag-Ce/γ-Al_2O_3 catalyst to effectively decompose O_3 and lead to generating more reactive species which are capable of destructing the VOCs molecules completely. Moreover, the presence of Ag-Ce/γ-Al_2O_3 catalyst in plasma significantly decreased the emission of discharge byproducts (NO_x and O_3) and promoted the mineralization of mixed VOCs towards CO_2. Adding a small amount of water vapor into PPC system enhanced the degradation efficiencies of mixed VOCs, however, further increasing water vapor had a negative impact on the degradation efficiencies, which was primarily attributed to the quenching of energetic electrons by water vapor in plasma and the competitive adsorption of water vapor on the catalyst surface. Meanwhile, the catalysts before and after discharge were characterized by the Brunauer-Emment-Teller and X-ray photoelectron spectroscopy.

1 Introduction

Volatile organic compounds (VOCs) in the atmosphere are one of the major environmental problems due to serious hazards to ecological system and adverse effects on public health. Non-thermal plasma (NTP) technology has been widely studied as a promising method for the abatement of dilute VOCs at ambient conditions since the past 20 years [1,2]. NTP process is featured by non-equilibrium, fast ignition, and low energy cost. Electrons generated in a

✉ Corresponding author
E-mail: lijie@dlut.edu.cn

sufficient strong electric field collide with molecules, producing photons, oxide icons, free radicals, high-energy electrons and metastable molecules. These species can initiate a series of chemical reactions, such as excitation, ionization and dissociation, leading to decompose VOCs efficiently [3,4]. Various types of the NTP processes have been investigated for the removal of VOCs, including pulsed streamer corona discharge [5,6], gliding arc discharge [7], ferroelectric pellet-packed bed discharge [8,9], and surface discharge [10]. In our previous study, an innovative plasma reactor, hybrid surface/packed-bed discharge (HSPBD) plasma reactor, has been proposed for benzene degradation, which showed better performance in benzene degradation efficiency, mineralization efficiency and energy yield than surface discharge reactor or packed-bed discharge reactor alone [11].

However, this NTP process alone has some inherent drawbacks such as low energy yield, poor CO_2 selectivity and undesirable byproducts. A synergy between NTP and heterogeneous catalysis is expected to be the best choice to overcome these technological drawbacks. Noble metal catalysts and transition metal catalysts have been studied deeply to promote VOCs degradation. Among them, Ag-based catalysts were reported to exhibit a high oxidizing capacity and good physical stability [12,13]. Cerium oxide (CeO_2) is known as a heterogeneous oxidation catalyst for the VOCs degradation reactions due to its excellent oxygen storage capacity (OSC) on the basis of the redox behavior between Ce^{3+} and Ce^{4+}. It can also act as a source of bulk oxygen species due to its labile oxygen vacancies and high oxygen mobility [14]. In recent years, compared to monometallic catalysts, bimetallic catalysts have gained increasing interest in the fields of combustion-catalysis and plasma-catalysis due to their multiple functionalities and excellent catalytic activity. The addition of Ce to Ag can facilitate the surface lattice of catalyst and increase the formation of surface adsorbed oxygen (O_{ads}), which plays a key role in the plasma-catalytic reactions and significantly improved pollutants degradation [15]. Nevertheless, very limited work has been carried out using the supported Ag-Ce catalysts in plasma-catalytic oxidation of mixture VOCs.

In general, there are two different types depending on the catalyst location: by being exposed to the active plasma volume (In Plasma Catalysis, IPC) [16,17] or by placing the catalyst downstream of the discharge zone (Post Plasma Catalysis, PPC) [18–20]. It has been noticed that although IPC and PPC processes both have good performance of the degradation of VOCs, IPC process can change the retention time of pollutants in the plasma reactor. Einaga et al. [21] reported that the degradation efficiency of benzene was higher 48% in PPC system (i.e. a DBD reactor and MnO_2 in series) than in NTP at the specific input energy of 180 $J \cdot L^{-1}$ and O_3 could vanish in PPC system. Zhu et al. [19] demonstrated that the maximum methanol removal efficiency of 95.4% using $Mn_{50}Ce_{50}$ oxide catalyst can be achieved in PPC system at a discharge power of 15 W and a gas flow rate of 1 L $\cdot min^{-1}$. In our previous research, it is found that PPC process was more effective at decomposing O_3 as well as destroying benzene than IPC system [22]. In addition, PPC system can also reduce the coke deposition to avoid the catalyst deactivation [23].

For industrial production, especially coating and chemical industries, various kinds of aromatic VOCs co-exists extensively and their emission has been limited strictly. The interaction between different kinds of VOCs in plasma-catalysis system is also fairly complex, and the synergistic mechanism study for mixed VOCs degradation is rather limited. Besides, from the view of industry application, gas relative humidity is also an important factor affecting the synergistic effect between plasma and catalysis as well as the energy utilization concerning VOCs degradation since VOCs emitted from industrial source generally contain water vapor.

In the present work, benzene, toluene and xylene were chosen as target pollutants and a PPC system was constructed by introducing the Ag-Ce/γ-Al_2O_3 catalyst downstream the discharge zone of the HSPBD plasma reactor. To understand the synergistic effects between plasma and catalysis, the degradation efficiencies, energy yields and CO_2 selectivities of the different single-component VOCs and mixed VOCs in both NTP and PPC processes were systematically discussed. FTIR was used to detect the decomposition products of single-component VOCs and mixed VOCs in NTP and PPC systems. In addition, the effects of the water vapor on the degradation efficiencies of mixed VOCs and O_3 concentration were also investigated.

2 Experimental

2.1 Experimental setup and apparatus

The schematic diagram of the experimental setup is shown in Fig. 1. It consists of a bipolar pulsed power supply (P60D-III, Institute of Special Power of DLUT, China), a reaction gas supply system, a hybrid surface/packed-bed discharge (HSPBD) plasma reactor, a post plasma catalyst reactor, an analytical system and a relative humidity regulating system. Benzene, toluene and xylene were put in water baths and evaporated by passing a pure nitrogen. The flow rates of nitrogen were controlled by three mass flow controllers (MFCs) (Sevenstar, China, 0–100 $mL \cdot min^{-1}$) to make sure the concentrations of VOCs accuracy. According to the different boiling point and saturated vapor pressure of three kinds of VOCs, the flow rates of nitrogen were 5.5, 7.1, and 9.2 $mL \cdot min^{-1}$ to obtain 100 ppm benzene, 100 ppm toluene and 100 ppm xylene, respectively. Three kinds of VOCs vapors were mixed with air completely and were fed into the reactor and then the

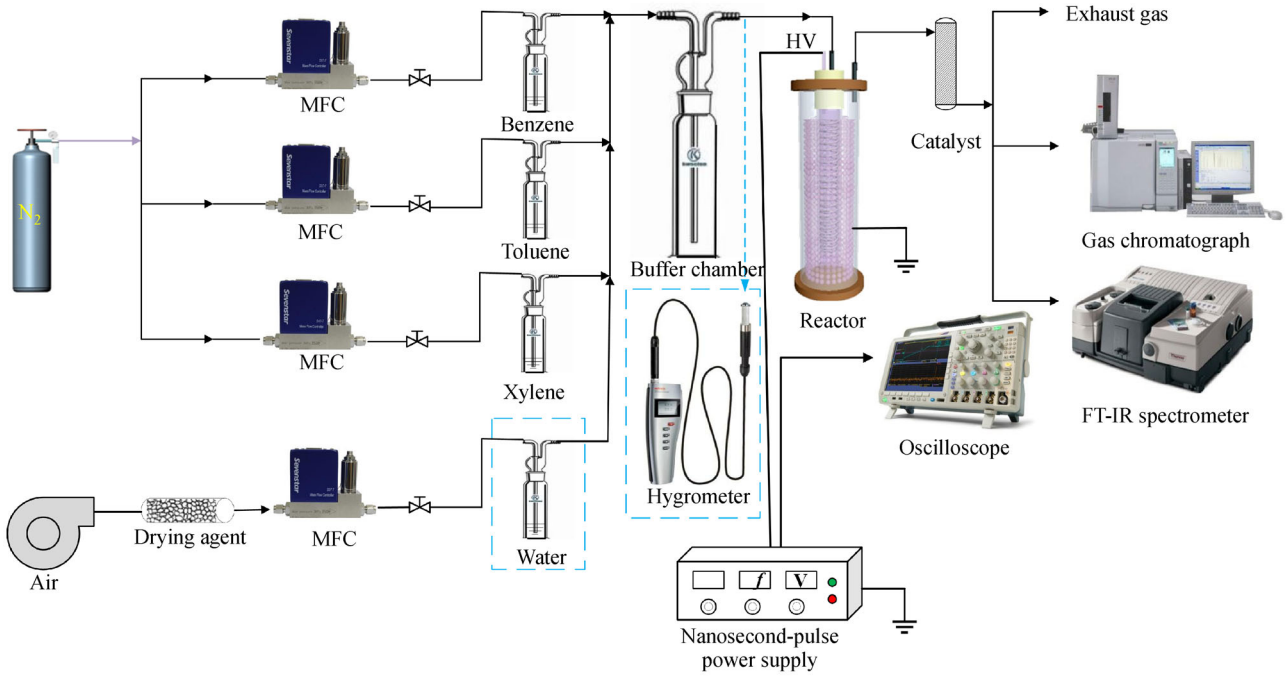

Fig. 1 Schematic diagram of the experimental setup

catalyst zone at standard temperature and pressure. The gas flow rate was fixed at 0.5 L·min^{-1} by using the mass flow controller (Sevenstar, China, 0–3 L·min^{-1}). The concentrations of VOCs at the inlet and outlet of reactor were analyzed by a gas chromatograph (Shimadzu GC-2010, Japan) equipped with a flame ionization detector (FID) and a 2 m Haysep-D packed column (GDX-102). The temperature program of the GC oven was the constant temperature 100°C. The inlet temperature and FID temperature were 65°C and 250°C, respectively. This condition was applied successfully to isolate and determine the benzene, toluene and xylene. Meanwhile, an online Fourier transform infrared spectroscopy (FTIR, Nicolet 6700, USA), equipped with a DTGS detector and a 2.4 m gas cell with KBr windows, was used to analyze the gaseous products. The O_3 concentration was measured by the iodometric method [24]. The concentrations of NO and NO_2 were measured by a flue gas analyzer (Testo 350, Germany). The electrical parameters were monitored with a four-channel digital oscilloscope (Tektronix TDS2024, USA), a voltage probe (Tektronix P6015A, USA) and a current probe (Tektronix P6021, USA). The relative humidity was adjusted by the dying agent and evaporable water content and tested by hygrometer (Rotronic 8303 Bassersdorf, Germany). The concentration of single-component VOC was 300 ppm, while mixed VOCs were comprised of 100 ppm benzene, 100 ppm toluene, and 100 ppm xylene.

2.2 Reactor configuration

A detailed description of the geometry of the plasma reactor has been published elsewhere [11]. Briefly, a 280 mm-long Plexiglas cylinder (i.d. 35 mm) and a 250 mm-long quartz tube (i.d. 14 mm) were used as the dielectric barrier in a coaxial configuration. The inner surface of Plexiglas cylinder was wrapped by an aluminum-foil (190 mm length) as the ground electrode. The inner discharge electrode was a roll of stainless-steel coil (1 mm diameter) around the inner surface of the quartz tube connected to the bipolar pulsed power. The open area between the Plexiglas cylinder and the quartz tube was filled with glass beads (3±0.3 mm). The residence time of the VOC components was 30 s. When a nanosecond pulsed voltage is applied between high-voltage electrode and ground electrode, surface discharge starts from the peripheral edges of the coil electrode and stretches out along the surface of dielectric barrier (the quartz tube), namely, surface discharge zone. At the same time, many microdischarges are generated at the contact points between the glass beads, namely, packed-bed discharge zone. The surface discharge and the packed-bed discharge occur concurrently in the reactor, thus, this type of plasma is considered as "hybrid plasmas." In addition, 3 g of Ag-Ce/γ-Al_2O_3 catalyst was introduced after the discharge zone and supported by Pyrex glass, which has an inner diameter of 1.5 cm and an effective length of 8.0 cm. The space velocity of the catalyst is 2062 h^{-1}.

2.3 Catalyst preparation and characterization

Ag-Ce/γ-Al_2O_3 (13.5 wt.% Ag and 1.5 wt.% Ce) was prepared by the impregnation method in this study based on previous experimental results [22]. The γ-Al_2O_3 pellets

of 2.5–3.5 mm in diameter as the support was first oxidized at 723 K for 2 h, followed by impregnation with silver nitrate and cerium nitrate aqueous solutions. Then it was dried at 378 K followed by calcination in air at 773 K for 5 h in the muffle furnace to obtain the catalyst. When the catalyst Ag-Ce/γ-Al_2O_3 was introduced in the discharge plasma system, the discharge was started after the outlet concentration was equal to the inlet concentration, which implied that the adsorption-desorption equilibrium was achieved over the catalyst surface to avoid the adsorption of catalyst to reduce the concentration of pollutants in degradation process. To compare the physico-chemical properties of the catalysts, the catalyst Ag/γ-Al_2O_3 (13.5 wt.% Ag) and Ce/γ-Al_2O_3 (1.5 wt.% Ce) were prepared in the same manner.

The Brunauer-Emment-Teller (BET) measurement was used to characterize the specific surface areas (S_{BET}) of the catalysts by carrying out a N_2 adsorption-desorption experiment at 77 K (Quantachrome Autosorb-1, America). The BET method was used to determine the total pore volume and the average pore diameter of the catalysts. X-ray photoelectron spectroscopy (XPS) spectra was recorded using a ThermoVG ESCALAN250 spectrometer fitted with Al-Kα source. High resolution (0.05 eV) was performed for photoelectron peaks at the pass energy of 20 eV to identify the chemical states of all the elements. All the binding energies were calibrated using the C1s neutral carbon peak at 284.65 eV as an internal standard. XPS data were processed by using the XPS Peak 4.1 software.

2.4 Methods

The energy (J) of a single pulse was determined by the applied voltage and current:

$$E_p = \int_0^t U_t \times i_t dt. \quad (1)$$

The average discharged power:

$$P = E_p \times f, \quad (2)$$

where U_t is the pulse voltage (V), i_t is the pulse current (A), t is time (s), E_p represents for energy delivered per pulse (J), f is the pulse frequency (Hz), P is discharge power (W).

The *SIE* was defined as the discharge power divided by the gas flow rate, which could be calculated with the following equations:

$$SIE(J/L) = \frac{P}{V} \times 60. \quad (3)$$

The energy yield (*EY*) as a measure of the energy efficiency was calculated as follows:

$$\eta_i = \frac{C_{inlet(i)} - C_{outlet(i)}}{C_{inlet(i)}} \times 100\%, \quad (4)$$

$$EY = \frac{3.6\Sigma C_{inlet(i)} \eta_i M_i}{22.4SIE}. \quad (5)$$

The selectivity of CO_2 was defined as follow:

$$S_{CO_2} = \frac{C_{outlet(i)[CO_2]}}{\Sigma n_i (C_{inlet(i)} - C_{outlet(i)})} \times 100\%, \quad (6)$$

where V is gas flow rate ($L \cdot min^{-1}$); $C_{inlet(i)}$ and $C_{outlet(i)}$ is the inlet concentration and outlet concentration of benzene, toluene or xylene (ppm), respectively; η_i is the conversion of benzene, toluene or xylene; and M_i corresponds to the molar mass of VOCs ($g \cdot mol^{-1}$); 22.4 is the molar volume of gas ($L \cdot mol^{-1}$) at the ambient condition; 60 and 3.6 are the unit conversion coefficients; $C_{outlet(i)[CO2]}$ is the outlet concentration of CO_2, i means one of the single-component or mixed VOCs; n_i is the number of carbon atoms in the molecules of benzene, toluene or xylene.

3 Results and discussion

3.1 Electric characterization of the discharge

The typical waveforms of applied voltage (U_t) and current (i_t) are shown in Fig. 2. When the HSPBD reactor was driven by bipolar nanosecond pulse power, the energy was injected into the discharge reactor in a very short moment (about 250 ns) and the peak value of current reached 200A at peak voltage 20 kV, so it can supply a very high instantaneous power 4×10^6 W. The duration time of a single pulse discharge was nearly 100 ns, which was much less than the time for gas heating or ionization instability (about10^5–10^6 ns) [25], therefore the input energy could generate a tremendous amount of high energy electrons and active species. In addition, an equivalent circuit of air gap in a HSPBD can be simulated using a variable resistor connected with a capacitance (C_g) in parallel, and then in series with a plane-parallel capacitor (C_d) [26]. According to the equivalent circuit, air gas current (i_g) (i.e. discharge current) and displacement current (i_d) were calculated by the formulae as follow. C_g and C_d were calculated by the simplified structure model [26]. The applied current (i_t) was the superposition of air gas current (i_g) and displacement current (i_d). It can be seen that gas current (i_g) takes up a great proportion in applied current, indicating that the input energy mainly used for the gas discharge to produce energetic electrons rather than energy consumption.

In addition, instantaneous discharge current presents multiple peaks in the primary discharge of the applied voltage for both polarity. For positive pulse, a first current peak occurs during the rise time of the voltage, which is due to the accumulation of the electrical charges produced by the discharge initiated close to the inner discharge

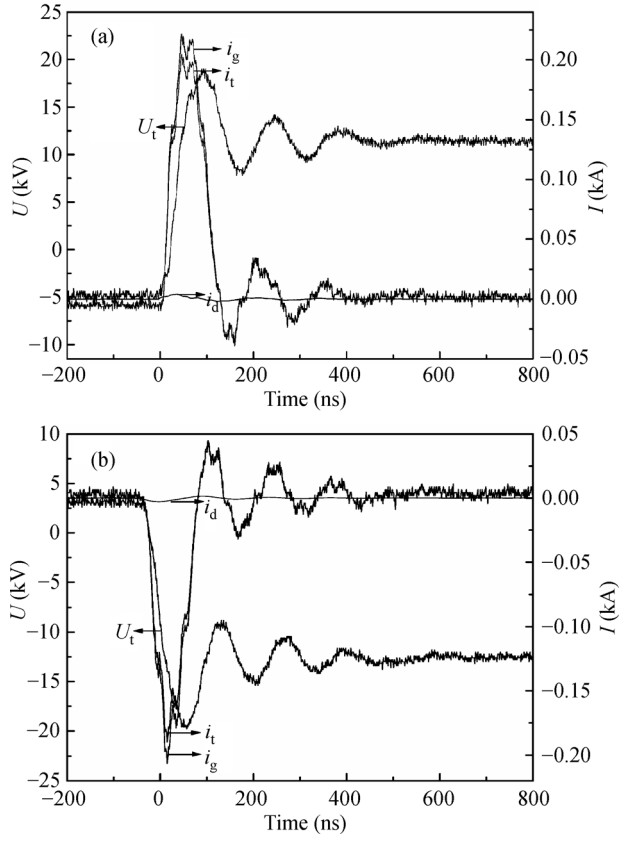

Fig. 2 Discharge voltage and current waveforms, gap current (i_g) and displacement current (i_d) of (a) the positive pulse and (b) the negative pulse

electrode where the electric field is intense enough. When the potential difference between the inner discharge electrode and the charged surface is adequate, a new discharge transmits on the dielectric layer, which results in the other discharge [27].

$$i_g = \left(1+\frac{C_g}{C_d}\right) i_t - C_g \frac{dU_t}{dt}, \quad (7)$$

$$i_d = \frac{C_g C_d}{C_g + C_d} \frac{dU_t}{dt}. \quad (8)$$

3.2 Catalyst characterization

Table 1 shows the surface area, total pore volume and average pore diameter of the support and the catalysts before and after discharge in the PPC process. Ag and Ce doping of the γ-Al_2O_3 cause a significant reduction in the surface area of catalysts. The S_{BET} of support γ-Al_2O_3 is 204.41 $m^2 \cdot g^{-1}$, while the S_{BET} of the Ag-Ce/γ-Al_2O_3 catalyst is about 160 $m^2 \cdot g^{-1}$. The pore volume of the catalysts is slightly lower than that of the support. The reduction in S_{BET} and pore volume for the Ag-Ce/γ-Al_2O_3 catalysts can be attributed to the coverage of γ-Al_2O_3 by Ag and Ce or partial occlusion of pores in the catalyst. In addition, the average pore diameters of catalysts are slightly larger than the support. Similar findings were reported by Zhu et al. using γ-Al_2O_3 supported single metal catalysts for the removal of acetone [28]. The average pore diameter (9.39 nm) of the Ag-Ce/γ-Al_2O_3 catalyst is enhanced compared to that Ag/γ-Al_2O_3 (8.89 nm) and Ce/γ-Al_2O_3 (8.76 nm), which could provide greater oxygen storage space for oxidation of VOCs. In addition, plasma exposure can result in the surface area of catalyst increase and the total pore volume decrease, indicating that ultrafine particles with higher specific surface area and crystal lattice with more vacancies have been formed. These physical changes could induce a higher catalytic activity, partially explaining the synergetic effect of plasma catalytic system [29].

To determine the chemical form of the atoms, the XPS spectra of Ag/γ-Al_2O_3, Ce/γ-Al_2O_3, Ag-Ce/γ-Al_2O_3 and Ag-Ce/γ-Al_2O_3 (after discharging 2 h) are shown in Fig. 3. As shown in Fig. 3(a), the XPS spectra of Ag 3d of all catalysts are symmetric and similar, which consisted of two individual characteristic peaks Ag $3d_{5/2}$ and Ag $3d_{3/2}$ at binding energy of 367.7 and 373.8 eV correspond to Ag^+ and Ag^0, respectively. Elemental Ag^0 can provide more atomic oxygen (Eq. (9)–(11)) [17], resulting in the adsorbed VOCs and intermediates on the catalyst surface more easily oxidized. In addition, it was observed that the peak intensity of the Ag $3d_{5/2}$ of Ag-Ce/γ-Al_2O_3 catalysts after discharge increases, indicating that the plasma promotes a higher degree of dispersion of metallic silver on the support.

Table 1 Physicochemical characteristics of the support and catalysts

Sample	Surface area ($m^2 \cdot g^{-1}$)	Total pore volume ($cm^3 \cdot g^{-1}$)	Average pore diameter (nm)
γ-Al_2O_3	204.41	0.4382	8.38
Ag/γ-Al_2O_3	167.99	0.3732	8.89
Ce/γ-Al_2O_3	197.08	0.4319	8.76
Ag-Ce/γ-Al_2O_3	162.22	0.3808	9.39
Ag-Ce/γ-Al_2O_3 (After discharging 2 h)	163.33	0.3720	9.11

$$2Ag + O_3 \rightarrow Ag_2O + O_2 \quad (9)$$

$$Ag_2O + O_3 \rightarrow Ag^{I}Ag^{III}O_2 + O_2 \quad (10)$$

$$O_3 \rightarrow O_2 + O_{ads} \quad (11)$$

The XPS spectra of Ce 3d of all samples are showed in Fig. 3(b), where u and indicate the spin-orbit splitting of states $3d_{3/2}$ and $3d_{5/2}$, respectively. XPS spectra can be divided into eight peaks by fitting the curves. The peaks labeled as υ' (885.7eV) and u' (903.7eV) are assigned to of Ce^{3+}, and the rest to Ce^{4+} [30]. As shown in Table 2, the concentration of Ce^{4+} are more than 60%, indicating that CeO_2 is the main chemical state of element Ce for the catalysts. It is found that the effect of the discharge plasma on the morphologies of the catalysts changed greatly and the concentration of CeO_2 was increased, indicating a strong interaction between Ag and Ce after discharging to promote the formation of CeO_2.

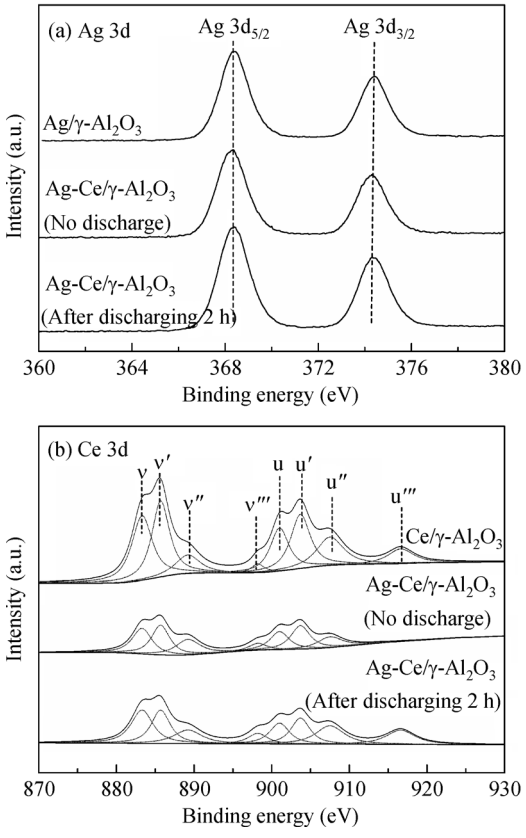

Fig. 3 XPS spectra of Ag /γ-Al_2O_3, Ce/γ-Al_2O_3, Ag-Ce/γ-Al_2O_3 and Ag-Ce/γ-Al_2O_3 (after discharging 2 h) (a) Ag 3d (b) Ce 3d

Table 2 Surface Ce element states of different catalysts

Sample	Surface Ce^{3+} (%)	Surface Ce^{4+} (%)
Ce/γ-Al_2O_3	38.47	61.63
Ag-Ce/γ-Al_2O_3	37.99	62.01
Ag-Ce/γ-Al_2O_3 (After discharging 2 h)	29.56	70.44

3.3 Comparison of single-component and mixed VOCs degradation in NTP and PPC processes

Figure 4 shows the degradation efficiencies of single-component VOCs and mixed VOCs as functions of *SIE* in NTP and PPC processes. The degradation efficiencies were measured after the discharge reached the steady-state, which means adsorption-desorption equilibrium of VOCs over the surface of catalyst to avoid the VOCs degradation by catalyst adsorption in PPC process. The result shows that the order of the degradation efficiencies was xylene>toluene>benzene in both single-component and mixed VOCs regardless of with or without catalyst. In PPC process, 98% of single-component xylene was degraded at 800 $J \cdot L^{-1}$, however, the corresponding degradation efficiencies of single-component toluene and benzene were 92% and 74%, respectively. This result is related to the stability of the molecular structure and the size of the molecular. The bond energies of the C_6H_5-CH_3, $C_6H_5CH_2$-H in toluene and xylene are 4.4 and 3.7 eV, respectively, which are significantly lower than the π bond in a benzene ring (5.0–5.3 eV) and C_6H_5-H bonds (4.9 eV) in benzene molecule [31]. On the other hand, the molecular size also

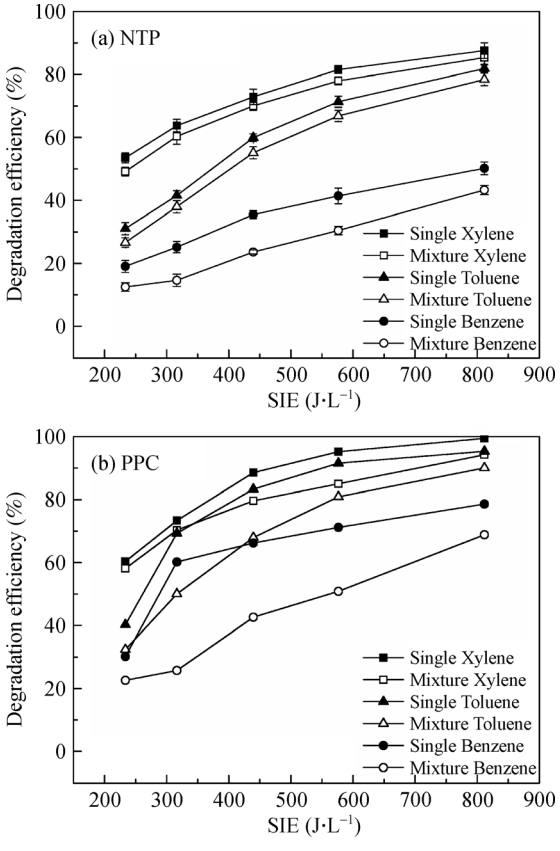

Fig. 4 The degradation efficiencies of single-component VOCs and mixed VOCs in NTP and PPC processes

influences the probability of collision because most reactions are initiated by inelastic collisions between aromatics and electrons and activated molecules, such as O and O_3 [31]. As a result, xylene is the most easily degradation component.

It can be observed that at the same *SIE*, the VOCs degradation efficiencies are higher in PPC process than in NTP process, suggesting that Ag-Ce/γ-Al_2O_3 has good catalytic performance for three kinds of pollutants. For example, the degradation efficiencies of mixed VOCs of benzene, toluene and xylene were 68%, 89% and 94% in PPC process at 800 J·L^{-1}, however, those were only 43%, 78% and 85% in NTP process. In PPC process, the active sites of the catalyst surface can decompose O_3 to generate the highly active species such as atomic oxygen and peroxide, which can decompose VOCs molecules more efficiently because the oxidation capacity of oxygen atom is much higher than O_3 [32]. It is also seen that the degradation efficiencies of the mixed VOCs are slightly lower than the single-component VOCs. The degradation efficiencies of benzene, toluene and xylene decreased by 7%, 3% and 2% respectively when they mixed together in NTP process at the *SIE* of 800 J·L^{-1}. This result might be attributed to the fact that more complex degradation intermediates generated in mixed VOCs consume more energy at the same *SIE*.

To study the catalytic properties of the bimetal catalyst for mixed contaminants further, the relations between outlet concentration and time were examined, as shown in Fig. 5. In the stage of catalytic adsorption, it can be seen that the outlet concentration of the three pollutants would return to the initial 100 ppm after a period of time in the absence of the plasma, indicating that the catalyst alone could not decompose VOCs at room temperature. The adsorption time of three pollutants in the mixture was different, which indicated that the adsorption capacities of the three kinds of pollutants were different. The order of adsorption capacity of the three pollutants was xylene>-toluene>benzene. However, the benzene concentration decreased rapidly and was adsorbed preferentially on the catalyst surface in the first five minutes of the adsorption cycle. The adsorption rate of benzene to the catalyst was the highest, which explained that compared with the NTP process, the degradation efficiency of benzene in the PPC process increased most.

3.4 Energy yields concerning single-component and mixed VOCs degradation in NTP and PPC processes

Figure 6 presents the energy yields concerning the decomposition of three kinds of single-component and mixed VOCs as a function of *SIE*. The energy yields increased first to the maximum and then decreased with the increase of *SIE*. This might suggest that input energy was utilized to degrade VOCs at lower *SIE* due to the more residual pollutants and the higher collision probability with the pollutant molecules at lower conversion. On the other hand, the concentration of VOCs decreased with the increase of VOCs degradation and hence the collision probability between the pollutant molecules and energetic species was lower at higher *SIE*. Meanwhile, a significant part of the input energy was converted into photons, heat, and used for byproducts formation at higher *SIE*. The order of the energy yield is xylene>toluene>mixture>benzene in both NTP and PPC processes. Comparing with the plasma only, the PPC process greatly improved the energy yields of VOCs. The energy yields of benzene, toluene and xylene were 2.3, 4.4 and 5.5 g·kWh^{-1} in NTP process, respectively, which increased to 3.4, 5.0 and 6.2 g·kWh^{-1} in PPC process at the *SIE* of 800 J·L^{-1}.

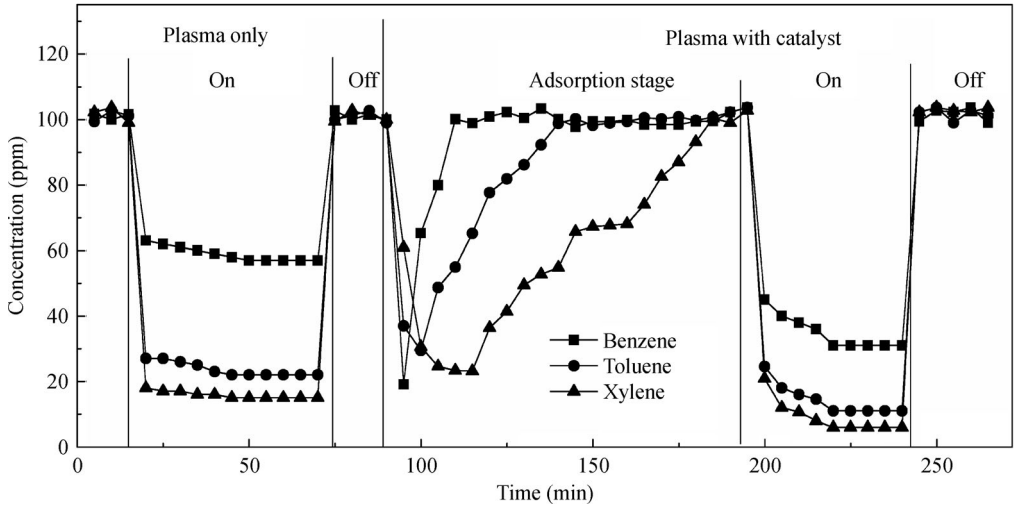

Fig. 5 The variation of the concentration of mixed VOCs with/without catalyst

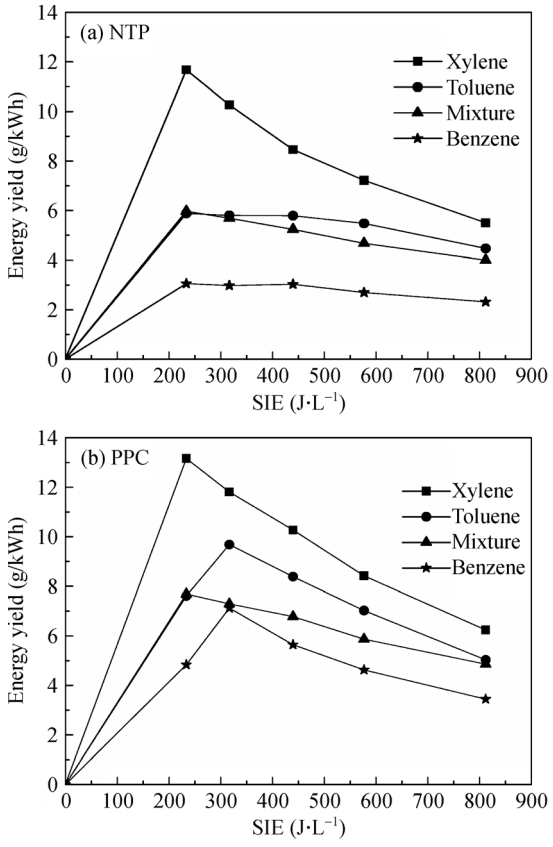

Fig. 6 Energy yield concerning single-component and mixed VOCs as a function of *SIE* in NTP and PPC systems

3.5 Behavior of products formation

3.5.1 Products analysis

The FTIR was used to analyze the decomposition and discharge products in gas phase after NTP and PPC treatments at the *SIE* of 800 J·L^{-1}, as shown in Fig. 7. The main gas products were C-containing products (CO_2, CO and HCOOH), discharge byproducts (N_2O, O_3) and H_2O. No other hydrocarbons except reactants and HCOOH were detected, suggesting that any other minor gaseous byproducts may be produced but they were at the sub-ppm level. As for xylene degradation, the absorption peak intensity of formic acid was stronger than benzene and toluene in NTP process, suggesting that formic acid can be produced by the approach, that is, the alkane fragments after benzene ring fracture and the methyl of benzene ring both can be further hydroxylated by the plasma consisted active substances ·OH, ·O and O_3. Compared to NTP process, the absorption peak intensities of CO, HCOOH and O_3 decreased, while the absorption peak intensities of CO_2 and H_2O increased in PPC process. These results indicate that the Ag-Ce/γ-Al_2O_3 after the plasma region plays an important role in the further oxidation of VOCs and by-products. VOC molecules and the intermediates can be adsorbed on the catalyst surface, and then converted to nontoxic CO_2 and H_2O via the active oxygen species of the catalyst surface. N_2O formed via reaction of NO with N [33], and its absorption peak intensity was lower in the existence of the catalyst due to competing reactions of NO with the active surface oxygen species. In addition, the absorption peak intensity of H_2O was stronger in PPC process than in NTP process, indicating that more VOC molecules and intermediates were completely oxidized in PPC process. The brown deposits on the tube wall were dissolved in methylene chloride, extracted by Rotary evaporator, and analyzed by GC-MS. The degradation products of the single-component are relatively simple, such as, phenol, benzaldehyde, benzoic acid, hydroquinone and heptanoic acid, while the deposit of the mixed VOCs contains some large molecular weight substance, such as bis(2-ethylhexyl) phthalate, phenanthrene, 3-ethenyl-3-methylcyclopentane, 1, 2-benzenediazonium and butyl phthalate.

3.5.2 CO_2 selectivities

CO_2 selectivity can directly reflect the mineralization degree of pollutants, thus quantitative analysis data for CO_2 is shown in Fig. 8 as a function of the *SIE*. It is seen that CO_2 selectivities in both NTP and PPC processes increased with the increase of *SIE* for all kinds of VOCs. For example, when the *SIE* increased from 234 J·L^{-1} to 800 J·L^{-1}, CO_2 selectivity of benzene increased from 29% to 72% in PPC process. This observation suggests that higher discharge power accelerates VOCs toward total oxidation. Compared to NTP process, O_3 can be decomposed to active oxygen atoms on catalyst surface active sites in PPC process, which can further oxide the intermediates to increase the concentration of CO_2. On the other hand, the residence time of intermediates can be extended effectively due to the catalyst adsorption characteristics, and thus the mineralization of intermediate products was accelerated. The CO_2 selectivity of different VOCs follows this sequence: benzene>mixture>toluene>xylene. Although the degradation efficiency of benzene was lower than of toluene or xylene, the intermediate products of benzene were more easily to be completely oxidized to the final products (CO_2 and H_2O) by energetic electrons and active particles. However, when methyl groups in toluene and xylene molecules fractured, they can be further decomposed into small molecular hydrocarbon organic products, which can also synthesize stable organic compounds such as biphenyl type macromolecule products.

3.5.3 The formation of NO_x

Formation of nitrogen oxides (NO and NO_2) is inevitable byproducts during the discharge, which are must be

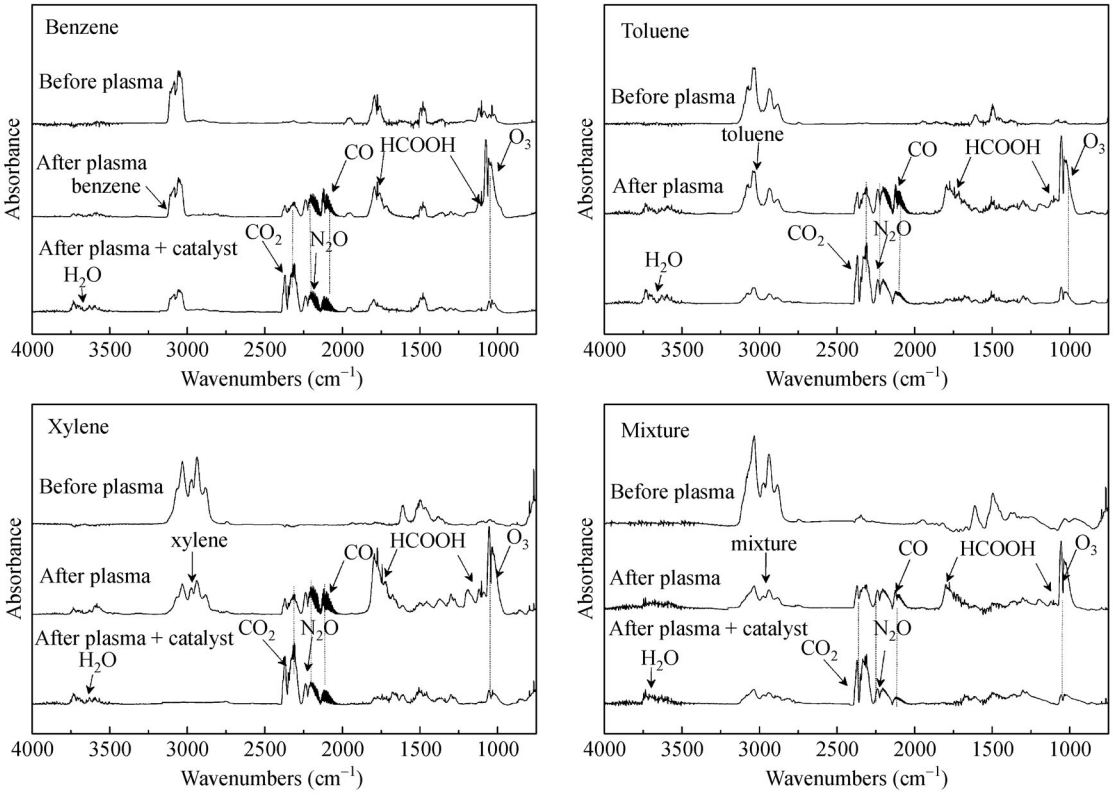

Fig. 7 FTIR spectra of gaseous products in hybrid surface/packed-bed discharge plasma reactor

characterized in the treatment process. Figure 9 shows NO_2 concentration as a function of the *SIE* in NTP and PPC processes. The major NO_x species monitored by the flue gas analyzer was NO_2, and there was no NO detected in both NTP and PPC processes because the HSPBD reactor is good source of O_3, which can oxidize efficiently NO toward NO_2 as Eq. (12):

$$O_3 + NO \rightarrow NO_2 + O_2$$

$$k = 1.8 \times 10^{-14} cm^3 molecule^{-1} s^{-1} \qquad (12)$$

It is seen from Fig. 9 that the concentration of NO_2 of single-component and mixed VOCs is approximately the same at the fixed *SIE* in both NTP and PPC processes. On the other hand, the NO_2 concentration is much lower in PPC process than in NTP process at the same *SIE*. For at the *SIE* of 800 $J \cdot L^{-1}$, the amount of NO_2 was 748 ppm in NTP process when mixed components were degraded, while only 170 ppm in PPC process. This could be attributed to the adsorption of NO_2 on the catalyst surface and then conversion to NO_3^- by active oxygen species. Similar findings also have been reported in previous works. Durme et al. [34] has detected NO_3^- on the catalyst surface by ion chromatography method during the decomposition of high-concentration O_3 generated by plasma discharge.

3.6 Effects of the relative humidity

3.6.1 Effects of the relative humidity on degradation efficiencies

Most of the industrial processes produce exhaust gases containing water vapor, so the effects of water vapor on the decomposition of VOCs should be carefully investigated. Figure 10 shows the effects of relative humidity on the decomposition of mixed VOCs in both NTP and PPC processes at 23 kV at a constant flow rate of 0.5 $L \cdot min^{-1}$. It was found that the degradation efficiencies first increased at lower relative humidity, then decreased with the further increased relative humidity. In PPC process, the degradation efficiencies of benzene, toluene and xylene enhanced from 65%, 84.5% and 96.6% to 68%, 86.5% and 98% as the relative humidity increased from 0 to 40%, while they decreased significantly to 54.8%, 74% and 88.3% at 100% relative humidity, respectively. This is because increasing the water vapor in gas phase can produce more energetic species such as ·H and ·OH (Eqs. (13)–(15)) to improve the degradation efficiencies. Among these species, ·OH is more active than other particles, such as oxygen and peroxide (Eqs. (16)–(20)) [35,36]. However, under the high relative humidity condition, the energetic electrons were attached by excess water molecules and thus the

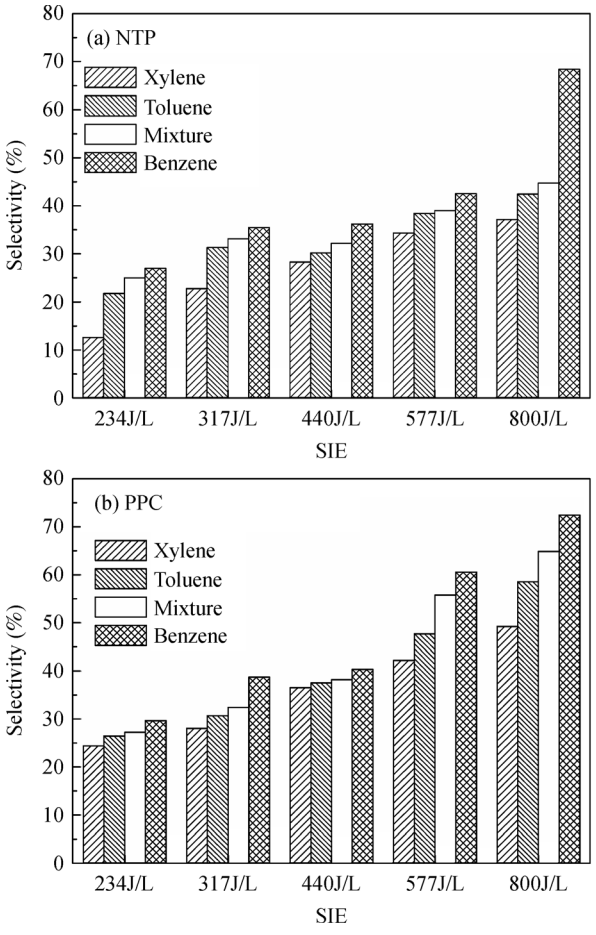

Fig. 8 CO_2 selectivities as a function of the *SIE* in NTP and PPC processes

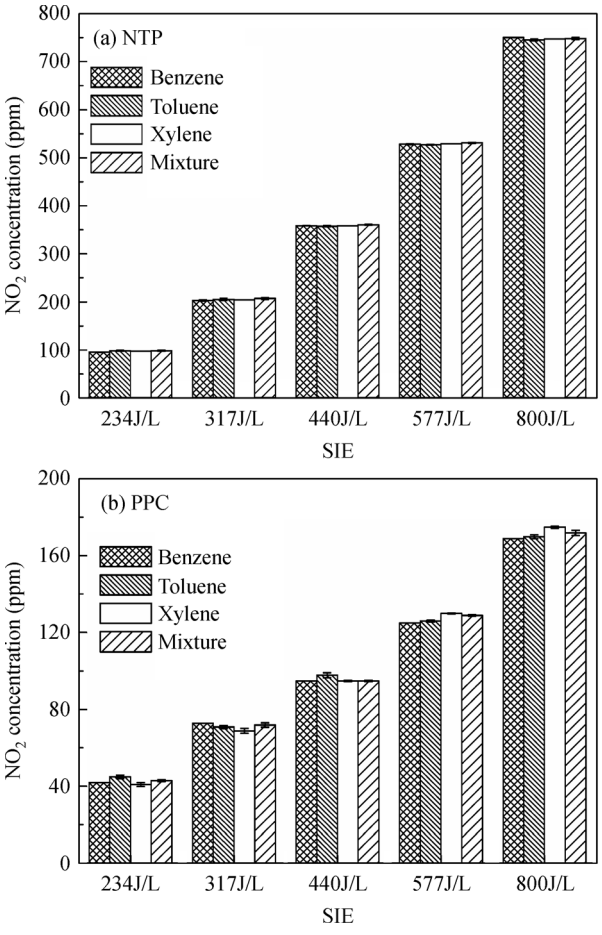

Fig. 9 NO_2 concentration as a function of the *SIE* in NTP and PPC processes

electron density in the discharge zone was reduced. Secondly, excess water molecules can occupy the active sites on the catalyst surface, which inhibited O_3 decomposition, and reduced the amount of VOCs adsorption on the surface of the catalyst.

$$H_2O + e^- \rightarrow \cdot OH + \cdot H + e^- \quad (13)$$

$$H_2O + N_2(A^3\Sigma_u^+) \rightarrow N_2 + \cdot OH + \cdot H \quad (14)$$

$$H_2O + O(^1D) \rightarrow 2\cdot OH \quad (15)$$

$$C_6H_6 + \cdot OH \rightarrow \text{products}$$

$$k_{298} = 1.2 \times 10^{-12} cm^3 molecule^{-1} s^{-1} \quad (16)$$

$$C_7H_8 + \cdot OH \rightarrow \text{products}$$

$$k_{298} = 5.7 \times 10^{-12} cm^3 molecule^{-1} s^{-1} \quad (17)$$

$$C_8H_{10} + \cdot OH \rightarrow \text{products}$$

$$k_{298} = 14.3 \times 10^{-12} cm^3 molecule^{-1} s^{-1} \quad (18)$$

$$C_6H_6 + \cdot O \rightarrow C_6H_5 + \cdot OH$$

$$k_{298} = 1.99 \times 10^{-14} cm^3 molecule^{-1} s^{-1} \quad (19)$$

$$C_7H_8 + O \rightarrow \text{products}$$

$$k_{298} = 2.32 \times 10^{-13} cm^3 molecule^{-1} s^{-1} \quad (20)$$

3.6.2 Effect of the relative humidity on O_3 formation

To understand the role of O_3 during the oxidation of mixture of VOCs, its concentration at the outlet was measured. Figure 10 also shows the O_3 outlet concentration as a function of relative humidity at 23 kV in NTP and PPC processes. The result shows that the O_3 concentration decreases as the relative humidity increased in NTP process, while increases in PPC process. In NTP process, O_3 outlet concentration was 3.0 $mg \cdot L^{-1}$ at the relative

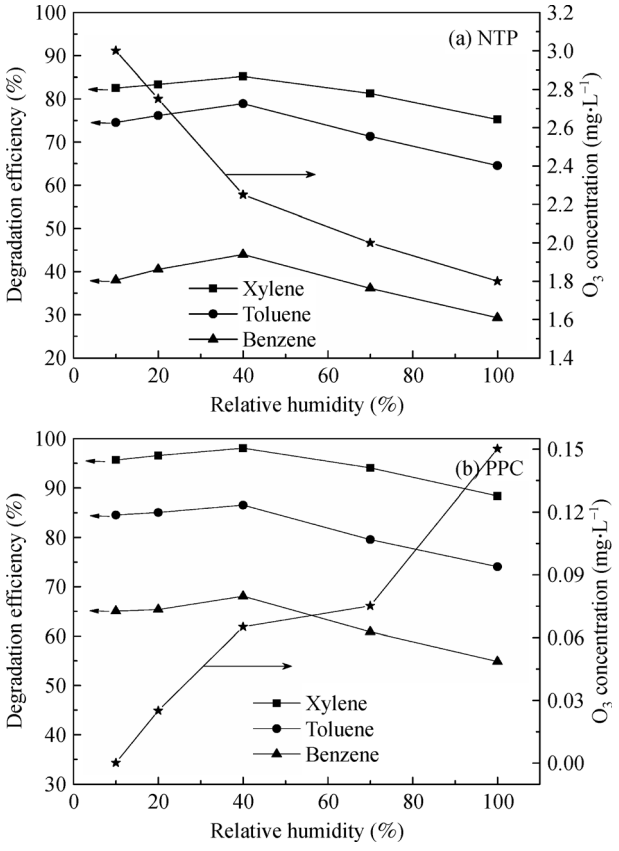

Fig. 10 Effects of the relative humidity on degradation efficiencies and O_3 concentration of mixed VOCs in NTP and PPC processes at 23 kV

humidity of 10%, which deceased to 1.8 mg·L^{-1} at 100% relative humidity. The lower of the O_3 concentration related to the electronegativity of water molecules, which limited the electron density and quenched activated chemical species, leading to generate fewer active particles. On the other hand, the discharge generated ·O reacted with H_2O, leading to the number of ·O decline dramatically and inhibit the generation of O_3.

Compare to NTP process, the introduction of the catalyst reduced the emissions of O_3 concentration due to O_3 catalytic decomposition on the Ag-Ce/γ-Al_2O_3 catalyst surface. In PPC process, O_3 concentration was 0 under 10% humid condition, while O_3 concentration increased to 0.15 mg·L^{-1} at the relative humidity of 100%. This result can be explained that the competitive adsorption between O_3 and H_2O molecules was occurred under high relative humidity condition, which limited the absorption of O_3 on the catalytic surface.

4 Conclusions

This study mainly focused on the degradation of mixed VOCs (benzene, toluene, and xylene) in PPC configuration using HSPBD plasma and Ag-Ce/γ-Al_2O_3 catalyst. The degradation efficiencies of three-component mixed VOCs were in the following order: xylene>toluene>benzene. This result can be attributed to the stability of the molecular structure and the size of the molecular. Compared with plasma-only process, the combined application of HSPBD plasma and Ag-Ce/γ-Al_2O_3 catalyst can lead to a significant enhancement in the degradation efficiencies of mixed VOCs. In PPC process, the degradation efficiencies of benzene, toluene, and xylene reached 68%, 89%, and 94% at the *SIE* of 800 J·L^{-1}, respectively, which were 25%, 11%, and 9% higher than those in plasma-only system. The CO_2 selectivities greatly improved when compared to the plasma-only system, thereby minimizing the formation of organic intermediates. Moreover, the emission of discharge byproducts (such as NO_x and O_3) was also inhibited in PPC system. Under low relative humidity (relative humidity < 40%) condition, the presence of water vapor has a significant positive impact on mixed VOCs degradation due to the generation of more energetic species. However, an obvious decrease can be observed in mixed VOCs degradation at high relative humidity, which can be ascribed to the quenching of active species and competitive adsorption of H_2O on the surface active sites of the catalyst. The optimal relative gas relative humidity is 40%.

Acknowledgements The authors thank the National Natural Science Foundation of China (Nos. 51507026 & 51177007), General Financial Grant from the China Postdoctoral Science Foundation (No. 2015M580223), Special Financial Grant from the China Postdoctoral Science Foundation (No. 2016T90221), and Dalian University of Technology Fundamental Research Fund (No. DUT15RC (3)030).

References

1. Chang M B, Lee C C. Destruction of formaldehyde with dielectric barrier discharge plasmas. Environmental Science & Technology, 1995, 29(1): 181–186
2. Chang J S. Recent development of plasma pollution control technology: A critical review. Science and Technology of Advanced Materials, 2001, 2(2): 571–576
3. Marotta E, Callea A, Rea M, Paradisi C. DC corona electric discharges for air pollution control. Part 1. Efficiency and products of hydrocarbon processing. Environmental Science & Technology, 2007, 41(16): 5862–5868
4. Aerts R, Tu X, Van Gaens W, Whitehead J C, Bogaerts A. Gas purification by nonthermal plasma: A case study of ethylene. Environmental Science & Technology, 2013, 47(12): 6478–6485
5. Mizuno A, Kisanuki Y, Noguchi M, Katsura S. Indoor air cleaning using a pulsed discharge plasma. IEEE Transactions on Industry Applications, 1999, 35(6): 1284–1288
6. Wang T C, Qu G Z, Yan Q H, Sun Q, Liang D, Hu S. Optimization of gas-liquid hybrid pulsed discharge plasma for *p*-nitrophenol contaminated dredged sediment remediation. Journal of Electro-

statics, 2015, 77: 166–173

7. Bo Z, Yan J, Li X, Chi Y, Cen K. Nitrogen dioxide formation in the gliding arc discharge-assisted decomposition of volatile organic compounds. Journal of Hazardous Materials, 2009, 166(2–3): 1210–1216
8. Liang W J, Li J, Li J X, Zhu T, Jin Y Q. Formaldehyde removal from gas streams by means of $NaNO_2$ dielectric barrier discharge plasma. Journal of Hazardous Materials, 2010, 175(1–3): 1090–1095
9. Yamamoto T, Tamanathan K, Lawless P A. Control of volatile organic compounds by an ac energized ferroelectric pellet reactor and a pulsed corona reactor. IEEE Transactions on Industry Applications, 1992, 28(3): 528–534
10. Jiang N, Guo L J, Shang K F, Lu N, Li J, Wu Y. Discharge and optical characterizations of nanosecond pulse sliding dielectric barrier discharge plasma for volatile organic compound degradation. Journal of Physics. D, Applied Physics, 2017, 50(15): 155206
11. Jiang N, Lu N, Shang K, Li J, Wu Y. Innovative approach for benzene degradation using hybrid surface/packed-bed discharge plasmas. Environmental Science & Technology, 2013, 47(17): 9898–9903
12. Tang X J, Feng F D, Ye L L, Zhang X, Huang Y, Liu Z, Yan K. Removal of dilute VOCs in air by post-plasma catalysis over Ag-based composite oxide catalysts. Catalysis Today, 2013, 211: 39–43
13. Einaga H, Ogata A. Catalytic oxidation of benzene in the gas phase over alumina-supported silver catalysts. Environmental Science & Technology, 2010, 44(7): 2612–2617
14. Zhu X B, Gao X, Qin R, Zeng Y, Qu R, Zheng C, Tu X. Plasma-catalytic removal of formaldehyde over Cu-Ce catalysts in a dielectric barrier discharge reactor. Applied Catalysis B: Environmental, 2015, 170-171: 293–300
15. Ding H X, Zhu A M, Lu F G, Xu Y, Zhang J, Yang X F. Low-temperature plasma-catalytic oxidation of formaldehyde in atmospheric pressure gas streams. Journal of Physics. D, Applied Physics, 2006, 39(16): 3603–3608
16. Oda T, Takahashi T, Kohzuma S. Decomposition of dilute trichloroethylene by using nonthermal plasma processing-frequency and catalyst effects. IEEE Transactions on Industry Applications, 2001, 37(4): 965–970
17. Karuppiah J, Reddy E L, Reddy P M, Ramaraju B, Karvembu R, Subrahmanyam Ch. Abatement of mixture of volatile organic compounds (VOCs) in a catalytic non-thermal plasma reactor. Journal of Hazardous Materials, 2012, 237–238: 283–289
18. Morent R, Dewulf J, Steenhaut N, Leys C, Van Langenhove H. Hybrid plasma-catalyst system for the removal of trichloroethylene in air. Journal of Advanced Oxidation Technologies, 2006, 9(1): 53–58
19. Zhu X B, Liu S Y, Cai Y X, Gao X, Zhou J, Zheng C, Tu X. Post-plasma catalytic removal of methanol over Mn-Ce catalysts in an atmospheric dielectric barrier discharge. Applied Catalysis B: Environmental, 2016, 183: 124–132
20. Fan X, Zhu T, Sun Y, Yan X. The roles of various plasma species in the plasma and plasma-catalytic removal of low-concentration formaldehyde in air. Journal of Hazardous Materials, 2011, 196 (196): 380–385
21. Einaga H, Ibusuki T, Futamura S. Performance evaluation of a hybrid system comprising silent discharge plasma and manganese oxide catalysts for benzene composition. IEEE Transactions on Industry Applications, 2001, 37(5): 1476–1482
22. Jiang N, Hu J, Li J, Shang K, Lu N, Wu Y. Plasma-catalytic degradation of benzene over Ag-Ce bimetallic oxide catalysts using hybrid surface/packed-bed discharge plasmas. Applied Catalysis B: Environmental, 2016, 184: 355–363
23. Chen H L, Lee H M, Chen S H, Chang M B, Yu S J, Li S N. Removal of volatile organic compounds by single-stage and two-stage plasma catalysis systems: A review of the performance enhancement mechanisms, current status, and suitable applications. Environmental Science & Technology, 2009, 43(7): 2216–2227
24. Birdsall C M, Jenkins A C, Spadinger E. Iodometric determination of ozone. Analytical Chemistry, 1952, 24(4): 662–664
25. Zhang S, Jia L, Wang W C, Yang D Z, Tang K, Liu Z J. The influencing factors of nanosecond pulse homogeneous dielectric barrier discharge in air. Spectrochimica Acta. Part A: Molecular and Biomolecular Spectroscopy, 2014, 117: 535–540
26. Mei D H, Zhu X B, He Y L. Plasma-assisted conversion of CO_2 in a dielectric barrier discharge reactor: understanding the effect of packing materials. Plasma Sources Science & Technology, 2015, (24): 015011
27. Aba'a Ndong A C, Zouzou N, Benard N. Geometrical optimization of a surface DBD powered by a nanosecond pulsed high voltage. Journal of Electrostatics, 2013, 71(3): 246–253
28. Zhu X B, Gao X, Yu X N. Catalyst screening for acetone removal in a single-stage plasma-catalysis system. Catalysis Today, 2016, (256): 108–114
29. Durme J V, Dewulf J, Leys C. Combining non-thermal plasma with heterogeneous catalysis in waste gas treatment: A review. Applied Catalysis B: Environmental, 2008, 78(3–4): 324–333
30. Skoda M, Cabala M, Matolinova I, Skála T, Veltruská K, Matolín V. A photoemission study of the ceria and Au-doped ceria/Cu(111) interfaces. Vacuum, 2009, 84(1): 8–12
31. Ogata A, Ito D, Mizuno K, Kushiyama S, Gal A, Yamamoto T. Effect of coexisting components on aromatic decomposition in a packed-bed plasma reactor. Applied Catalysis A, General, 2002, 236 (1–2): 9–15
32. Futamura S, Zhang A, Einaga H, Kabashima H. Involvement of catalyst materials in nonthermal plasma chemical processing of hazardous air pollutants. Catalysis Today, 2002, 72(3–4): 259–265
33. vanVeldhuizen E M. Electrical Discharges for Environmental Purposes: Fundamentals and Applications. New York: Nova Science Publishers, 2000
34. Durme J V, Dewulf J, Sysmans W, Leys C, Langenhove H V. Efficient toluene abatement in indoor air by a plasma catalytic hybrid system. Applied Catalysis B: Environmental, 2007, 74(1–2): 161–169
35. Cvetanovic R J. Evaluated chemical kinetic data for the reactions of atomic oxygen $O(^3P)$ with understand hydrocarbons. Journal of Physical and Chemical Reference Data, 1987, 16(2): 261–321
36. Lias S G. Ionization energy evaluation, In: NIST Standard Reference Database. Maillard W G, Linstrom P J, eds. National Institute of Standard and Technology, Gaithersburg, MD, 2006